Partial Differential Equations in Applied Mathematics 13 (2025) 101109

Contents lists available at ScienceDirect

Partial Differential Equations in Applied Mathematics

journal homepage: www.elsevier.com/locate/padiff

Modeling the flow of casson nanofluid on a stretching sheet with heat transfer: A study of electric MHD and Darcy-Forchheimer effects

Hamzeh Taha Alkasasbeh

Department of Mathematics, Faculty of Science, Ajloun National University, P.O. Box 43, Ajloun 26810, Jordan

ARTICLE INFO

Keywords:
Electric MHD
Darcy-forchheimer
Casson fluid
Nanofluid
Stretching sheet
Convective Boundary Conditions

ABSTRACT

This article investigates the flow characteristics of Casson-type nanofluid, specifically focusing on its behavior under Darcy-Forchheimer conditions over a stretching sheet with convective boundary conditions, which have significant implications across various fields, particularly in engineering and biomedical applications. Understanding this flow is crucial due to its applications in various industrial processes, such as cooling systems, material processing, and biomedical engineering, where efficient heat transfer and fluid dynamics are essential. The study primarily examines the electric magnetohydrodynamic (MHD) flow of copper oxide suspended in water, forming a Casson nanofluid. This research is significant as it contributes to the optimization of cooling techniques and enhances the performance of materials in high-temperature applications. The transformation of the governing partial differential equations (PDE) into ordinary differential equations (ODE) allows for a more manageable analytical approach, facilitating numerical solutions through MATLAB's bvp4c function. The findings reveal that pure water exhibits a greater velocity and Nusselt number compared to the copper oxide-based Casson nanofluid. Conversely, the temperature and skin friction coefficient demonstrate an inverse relationship. These insights are essential for designing more effective thermal management systems, improving energy efficiency in manufacturing processes, and advancing technologies that rely on nanofluid dynamics.

Nomenclature

B Casson Parameter
B_i Biot number
Cf Local Skin Friction Coefficient,
c_p Specific Heat Capacity, $Jkg^{-1}K^{-1}$
Da Darcy Number
E Electric Parameter
Ec Eckert Number
ϱ_{ij} Deformation rate W m^{-2} K^{-1}
h_f Heat transfer coefficient $Wm^{-2}K^{-1}$
M Magnetic Parameter
k Thermal conductivity $Wm^{-1}K^{-1}$
Nu Nusselt Number
p_y Yield stress N m^{-2}
Pr Prandtl Number
Re Local Reynolds Number.
T Temperature,
u_w Variable Shrinking Velocity, Ms^{-1}
u Velocity Component Along x-axis, Ms^{-1}
v Velocity Component along y-axis, Ms^{-1}
β_o Strength of magnetic field
μ Dynamic Viscosity, $Kgm^{-1}s^{-1}$
μ_m Plastic Dynamic
k Kinematic Viscosity, M^2s^{-1}
ρ Density, Kgm^{-3}
σ Electrical Conductivity, $A^2s^3kg^{-1}m^{-3}$
ψ Stream Function, $Kgm^{-1}s^{-1}$
τ Shear Rate, $Kgm^{-1}s^{-2}$
ζ_{ij} Stress tensor N m^{-2}
π Critical Value
χ Nanoparticle Volume Fraction

Subscripts

f base fluid
nf anofluid
w Wall/Surface
∞ Ambient Environment

E-mail address: alkasasbehh@anu.edu.jo.

https://doi.org/10.1016/j.padiff.2025.101109
Received 20 September 2024; Received in revised form 18 December 2024; Accepted 1 February 2025
Available online 2 February 2025

1. Introduction

Non-Newtonian fluids, such as Casson fluid, are of significant interest in various industries and applications, including chemical processing, plastics manufacture, mining, tissue engineering, the pipeline industry, biomedical transport, and lubrication. These fluids exhibit complex behavior, and their viscosity is not a fixed scalar but a variable, making their simulation challenging. Engineers and scientists often work with Newtonian fluids like air, water, and oil, but the need to simulate non-Newtonian fluid flow arises in many real-world scenarios. For instance, in the biomedical field, the study of non-Newtonian properties of blood is crucial for simulating blood flow in arteries.[1] The viscosity of non-Newtonian fluids, including Casson fluid, depends on various factors such as shear rate and temperature, and accurate simulation of their flow behavior is essential for many practical applications.[2] Casson[3] developed a fluid model to describe the behavior of non-Newtonian fluids with yield stress, and it has found applications in studying blood flow, the paint industry, medicine manufacturing, synthetic lubricants, and other areas.

The simulation of non-Newtonian fluid flow is a complex and crucial task in various industries and fields. The behavior of these fluids, such as Casson fluid, is significantly different from that of Newtonian fluids, and their viscosity is a variable rather than a fixed scalar. Therefore, the development of accurate simulation models for non-Newtonian fluid flow is essential for understanding and predicting their behavior in practical applications.[4-6] Nanofluids outperform conventional carrier liquids in terms of thermal performance, and they have practical applications in a variety of thermal engineering processes such as fuel cells, refrigerators, and engine oil. Choi and Eastman[7] study, which added nano-sized metallic particles to carrier fluids, concluded that thermal features improved significantly. Nanofluids have been used in various applications, including heat pipes, heat exchangers, automobile radiators, solar energy systems, and electronic chips.[8] In heat pipes, nanofluids have demonstrated higher thermal performance of up to 70 W compared to water as a base fluid.[9] Kaggwa, et al.[10] have also been used the nanofluids in parabolic trough solar concentrators, where they can increase the overall thermal performance by up to 1–2%. The electromagnetic hydrodynamic (EMHD) effect on nanofluid flow has been the subject of several research studies. These studies have investigated the behavior of nanofluids under the influence of electromagnetic forces, and the results have implications for various applications. Irfan et al.[11] presented a computational technique for EMHD nanofluid flow, establishing mathematical models for constant and variable fluid flows. A study by Algehyne et al.[12] examined the EMHD flow of a zinc-oxide–-water nanofluid past a bidirectional Riga plate, considering velocity slips and convective boundary conditions. Ali et al.[13] investigated the effects of nanofluid flow over a non-linear stretchable surface, considering variables such as radiation, heat flux, viscosity, and Joule heating. The stability analysis of Casson nanofluid on a stretching sheet has been the subject of several research studies such as Lanjwani et al[14, 15] who considered the (MHD) two-dimensional boundary layer flow of Casson nanofluid on an exponential stretching/shrinking sheet with the effects of radiation and focused on the stability analysis of incompressible steady-state 2D stratified boundary-driven Casson nanofluid flowing over a stretched/shrunk surface. Basha and Sivaraj[16] discussed a numerical study scrutinizes the dual solutions and stability analysis of the flow of Casson nanofluid past a permeable surface. Moreover, El-Zaharet al.[17] showed that unsteady MHD mixed convection flow is examined for a non-Newtonian Casson hybrid nanofluid stagnating in a rotating sphere as a result of impulsive motion between the angular velocity of the sphere and the velocity of the free stream in the stagnation zone.

The Darcy-Forchheimer model, which describes fluid flow through porous media, has been extended to include magnetohydrodynamics (MHD) and electric effects in various applications, such as nanofluids and heat transfer. Several research studies have investigated the influence of the Darcy-Forchheimer relation on MHD dissipative third-grade fluid flow and heat transfer in porous media, as well as on nanofluid flow with heating and dissipation effects over various geometries.[18-20] Jawad et al[21] analyzed the magnetohydrodynamic laminar flow past a vertical permeable surface using the Darcy-Forchheimer model. Shuguang et al.[22] presented the impacts of activation energy and chemical reaction on the magnetohydrodynamic Darcy-Forchheimer squeezed Casson fluid flow over a horizontal channel. Butt et al[23] investigated numerically observes the electro-magneto impacts during Darcy-Forchheimer viscous fluid flow with a nonlinear form. The solution for nanofluid flow stretching when the MHD electrical effect is executed with ohmic heating was performed by Lund et al. .[24] Abbas et al.[25] shown the influence of the Darcy-Forchheimer relation on third-grade fluid flow and heat transfer over a porous medium with Joule heating effects using a numerical approach. The Darcy-Forchheimer flow of Casson nanofluids (Buongiorno nanofluid model) across a stretching sheet is investigated by Hafez et al. .[26] An impermeable horizontal cylinder was convectionated through non-Darcy natural convection with a combined magnetohydrodynamic heat and mass transfer problem under coupled thermal and mass diffusion, inertia resistance, magnetic field, thermal radiation effects in a porous medium under non-Newtonian power law fluid embedded in porous medium by El-Kabeir et al. .[27] The effect of magnetic field on free convection along a vertical plate in a thermally stratified nanofluid saturated non-Darcy porous medium has been studied by Murthy et al. .[28]

The current study addresses a significant gap in the existing literature by exploring the electric magnetohydrodynamic (EMHD) Darcy-Forchheimer flow of Casson nanofluid, specifically copper oxide suspended in water, over a stretching sheet with convective boundary conditions. This topic is important due to the increasing applications of nanofluids in various industries, including cooling systems, energy production, and biomedical technologies, where enhanced thermal performance is critical. Despite the extensive research on nanofluids, the specific dynamics of EMHD flow under Darcy-Forchheimer conditions have not been previously investigated. By employing the MATLAB bvp4c solver to numerically solve the dimensionless nonlinear coupled governing equations, this study provides a novel contribution to the understanding of how velocity distribution and temperature profiles are affected by various parameters.The findings reveal that the temperature distribution improves with increasing heat generation parameters, which is crucial for optimizing thermal management in engineering applications. Additionally, this research validates its results through comparisons with published studies, enhancing the credibility of the findings. The creation of tables detailing Nusselt numbers and skin friction coefficients across different parameters and fluid types further contributes to the body of knowledge in this field. Overall, this study not only fills a critical research gap but also offers valuable insights that can inform future applications and advancements in nanofluid technology and thermal management systems.

2. Mathematical formulation

Take a steady the incompressible 2D Darcy-Forchheimer flow of Casson nanofluid, specifically Copper oxide (CuO) with water (H_2O) as base fluid and pure water across a stretched stretching sheet in the context of electro-magnetohydrodynamic (EMHD) flow. The Darcy-Forchheimer flow effect has significance in areas such as petroleum engineering, where the high flow rate impact is common. Furthermore, porous media are employed in a wide range of operations, including geophysical design, heat transmission, and others. Energy storage systems, solar receivers, and a variety of other equipment are also vulnerable. Regardless of the magnetic force's implemented characteristics, the nanoparticles are electrically conductive. On the sheet, the magnetic field $\beta = (0, \beta_0, 0)$ is functioning naturally.

The fluid conducts electricity, and the applied magnetic field gen-

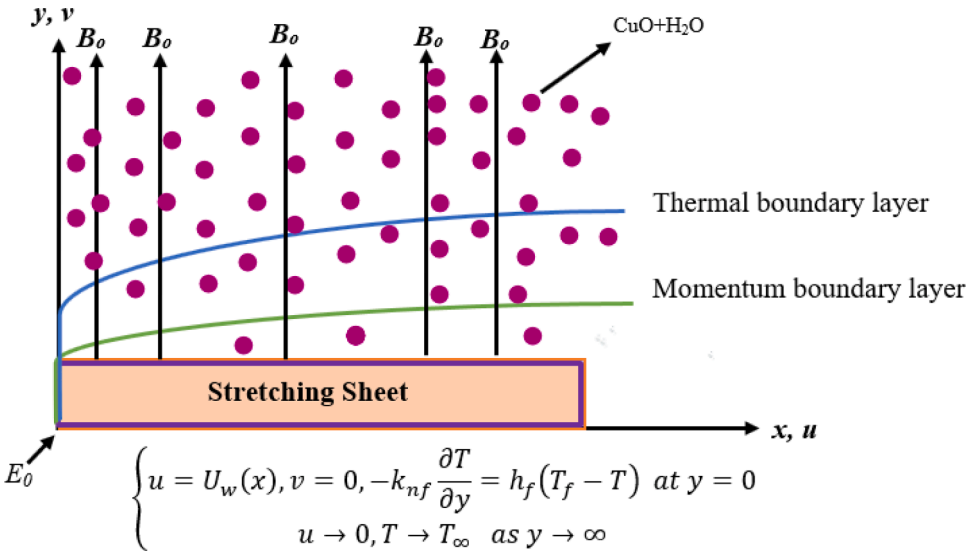

Fig. 1. Flow model of CuO+H_2O Casson nanofluid.

erates the electric field $E = (0, 0, E_0)$ The surface was expanded using convective boundary conditions at $U_w(x) = ax,\ a > 0$.The y-axis was normal to the stretchable surface, and the x-axis was parallel to it, as shown in Fig. 1.The leading boundary layer equation for the boundary condition and the flow of fluid assumptions.

The Casson fluid flow has been explored as follows[3] .

$$\zeta_{ij} = \begin{cases} 2\left(\mu_m + p_y \Big/ \sqrt{2\pi}\right)\varrho_{ij} & \pi > \pi_c, \\ 2\left(\mu_m + p_y \Big/ \sqrt{2\pi_c}\right)\varrho_{ij} & \pi < \pi_c \end{cases} \tag{1}$$

where ζ_{ij}, ϱ_{ij}, μ_m, and p_y are respectively, stress tensor, deformation tensor, plastic dynamic viscosity and yield stress of the Casson fluid. Further, π denoted the multiplication of the component of the deformation rate, π_c is the critical value.

According to aforementioned suppositions, governing equations with boundary conditions can be expressed as[26]:

$$\frac{\partial u}{\partial x} + \frac{\partial v}{\partial y} = 0, \tag{2}$$

$$\begin{cases} u = U_w(x),\ v = 0,\ -k_{nf}\dfrac{\partial T}{\partial y} = h_f(T_f - T)\ at\ y = 0, \\ u \to 0,\ T \to T_\infty\ as\ y \to \infty\ . \end{cases} \tag{5}$$

The following table enumerates the characteristics of nanofluids[5,6]:

The following similarity transformations are used to convert PDEs to ODEs[26]:

$$\psi(x,y) = -\sqrt{av}xf(\eta),\ \theta(\eta) = \frac{T - T_\infty}{T_f - T_\infty},\ \eta = \sqrt{\frac{a}{v_f}}y. \tag{6}$$

Eq. (2) is instantly satisfied when the previously stated relations are applied and Eqs. (3) and (4) are condensed dimensionless to

$$\varphi_2\left(1 + \frac{1}{B}\right)f''' + \varphi_1(ff'' - f'^2) + \varphi_3 M(E - f') - F_s f'^2 - \frac{\varphi_2}{Da}f' = 0, \tag{7}$$

$$\varphi_5\theta'' + \Pr\varphi_4 f\theta' + \varphi_3 M(Ec)(f' - E)^2 + \varphi_2 \Pr(Ec)\left(1 + \frac{1}{B}\right)f'^2 = 0, \tag{8}$$

where

$$\varphi_1 = (1-\chi) + \chi\left(\frac{\rho_s}{\rho_f}\right),\quad \varphi_2 = (1-\chi)^{-2.5},$$
$$\varphi_3 = 1 + \left[\frac{3(\sigma-1)\chi}{(\sigma+2) - (\sigma-1)\chi}\right],\quad \varphi_4 = (1-\chi) + \chi\frac{(\rho C_p)_s}{(\rho C_p)_f},\quad \varphi_5 = \frac{(k_s + 2k_f) - 2\chi(k_f - k_s)}{(k_s + 2k_f) + \chi(k_f - k_s)}, \tag{9}$$

$$u\frac{\partial u}{\partial x} + v\frac{\partial v}{\partial y} = V_{nf}\left(1 + \frac{1}{B}\right)\frac{\partial^2 u}{\partial y^2} + \frac{\sigma_{nf}}{\rho_{nf}}(E_0\beta_0 - \beta_0^2 u) - \frac{V_{nf}}{K^*}u - \frac{F}{\sqrt{K^*}}u^2, \tag{3}$$

$$u\frac{\partial T}{\partial x} + v\frac{\partial T}{\partial y} = \frac{k_{nf}}{(\rho C_p)_{nf}}\frac{\partial^2 T}{\partial y^2} + \frac{\sigma_{nf}}{(\rho C_p)_{nf}}(E_0\beta_0 - \beta_0^2 u)^2 + \frac{\mu_{nf}}{(\rho C_p)_{nf}}\left(1 + \frac{1}{B}\right)\left(\frac{\partial u}{\partial y}\right)^2. \tag{4}$$

With BCs

and $M = \frac{\sigma_f\beta_0^2}{a\rho_f}$ is magnetic parameter, $E = \frac{E_o}{U_w\beta_0}$ is electric paremeter, $F_s = \frac{F}{\sqrt{K^*}}x$ is Forchheimer number, $Da = \frac{aK^*}{v_f}$ is the Darcy number, $Pr = \frac{(\rho C_p)_f}{k_f}$ is Prandtl number, $Ec = \frac{U_w^2}{(\rho C_p)_f(T_f - T_\infty)}$ is the Eckert number, $E = \frac{E_o}{U_w\beta_0}$ is electric paremeter and B is Casson paremeter.

The non-dimensional boundary conditions (5) are as follows:

$$\begin{aligned} &f = 0, f' = 1,\ \theta' = Bi(1 - \theta)\ \ \text{at}\ \ \eta = 0, \\ &f' \to 0,\ \ \theta \to 0,\ \ as\ \eta \to \infty. \end{aligned} \tag{10}$$

Here $B_i = \frac{h_f}{k_f}\sqrt{\frac{v_f}{a}}$ is the Biot naumber.

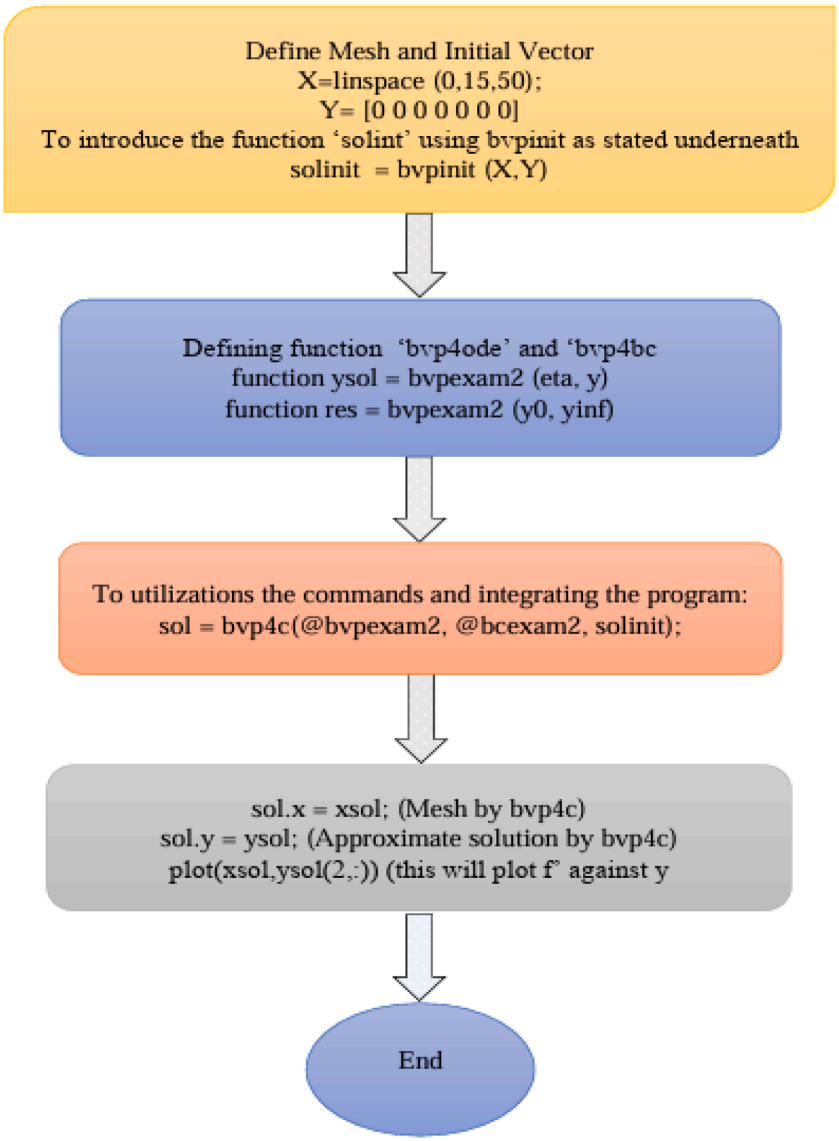

Fig 2. Flow chart of bvp4c method.

Table 1

Properties	Nanofluid
μ Viscosity	$\mu_{nf} = \frac{\mu_f}{(1-\chi)^{2.5}}$
ρ Density	$\rho_{nf} = (1-\chi)\rho_f + \chi\rho_s$
(ρC_P) Heat capacity	$(\rho C_p)_{nf} = (1-\chi)(\rho C_p)_f + \chi(\rho C_p)_s$
k Thermal conductivity	$\frac{k_{nf}}{k_f} = \frac{(k_s+2k_f)-2\chi(k_f-k_s)}{(k_s+2k_f)+\chi(k_f-k_s)}$
σ Electrical conductivity	$\sigma_{nf} = \sigma_f\left[1+\frac{3(\sigma-1)\chi}{(\sigma+2)-(\sigma-1)\chi}\right],\ \sigma = \frac{\sigma_s}{\sigma_f}$

The dimensionless physical quantities of importance are the skin friction coefficient Cf and the Nusselt number Nu which are expressed mathematically as:

$$Cf = \left(1+\frac{1}{B}\right)\frac{\mu_{nf}}{U_w^2\rho_f}\left(\frac{\partial u}{\partial y}\right)_{y=0},\ Nu = \frac{xk_{nf}}{k_{f(T_f-T_\infty)}}\left(\frac{\partial T}{\partial y}\right)_{y=0}. \tag{11}$$

The non-dimensional skin friction coefficient and Nusselt number obtained by applying (6) in (11), are as follows:

$$Re_x^{\frac{1}{2}}Cf = \varphi_2\left(1+\frac{1}{B}\right)f''(0), Re_x^{-\frac{1}{2}}Nu = -\varphi_5\theta'(0). \tag{12}$$

Table 2
Compared value of Da on $-f''(0)$ *and* $-\theta'(0)$ when $Ec = 0.1, Fs = 10, \Pr = 6, Bi = 0.3$, $M = 0.1$, $E = 0.1$ and $\chi = 0$.

	Hafez et al.[26]		Present	
Da	$-f''(0)$	$-\theta'(0)$	$-f''(0)$	$-\theta'(0)$
2.1	4.90451027642328	0.470876163357646	4.904510276424381	0.470876163213145
2.2	4.78638341938640	0.471775614053540	4.786383419376210	0.471775614121451
2.3	4.67633131612419	0.472629890538819	4.676331316152212	0.472629890496210
2.4	4.57351158496662	0.473442398930219	4.573511584959631	0.473442398900124

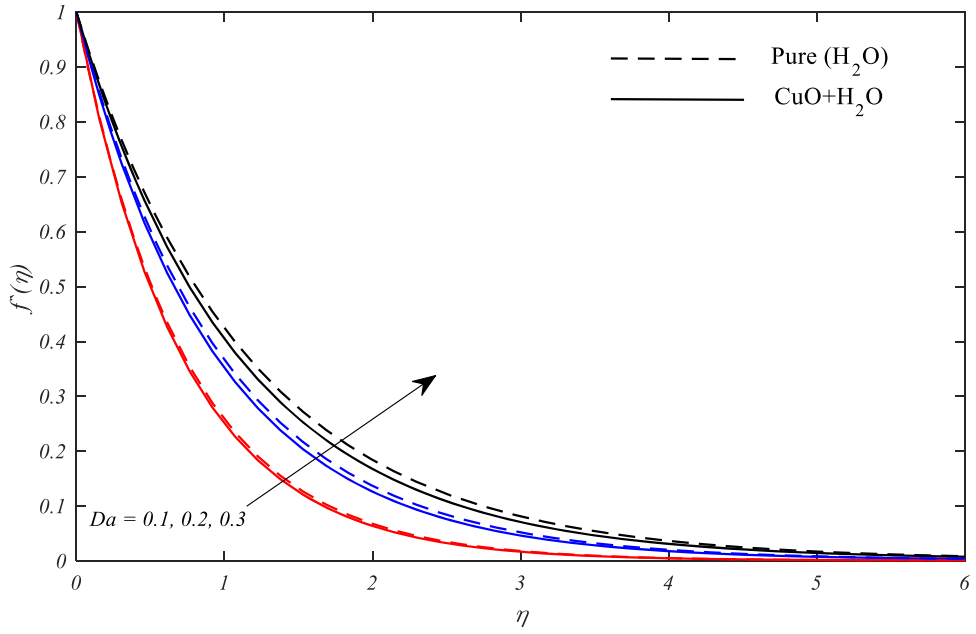

Fig. 3. Variation of $f'(\eta)$ vs. *Da*.

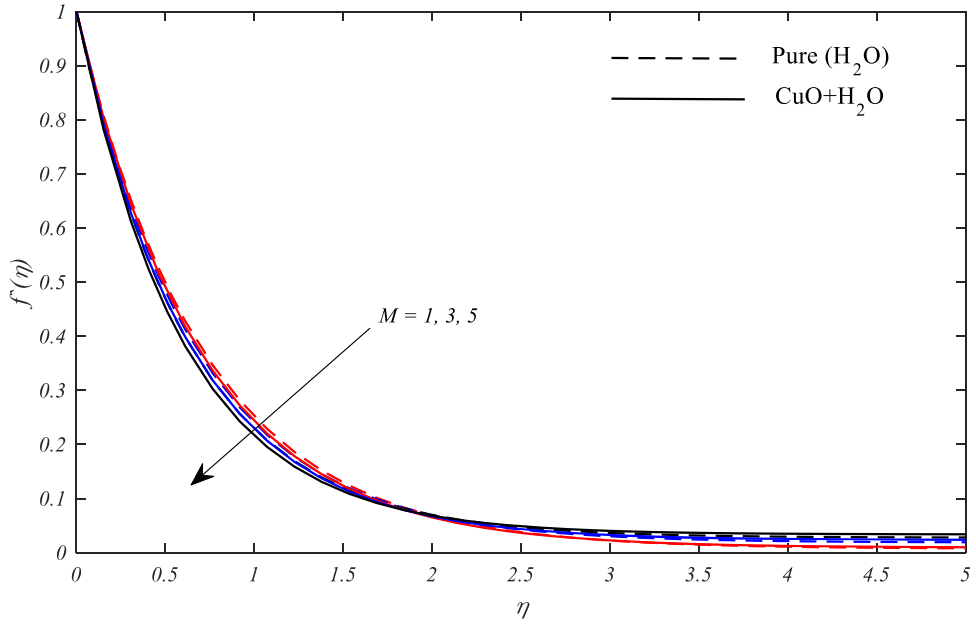

Fig. 4. Variation of $f'(\eta)$ vs. *M*.

3. Numerical approach

We achieved numerical results for CuO+H_2O and pure water with MATLAB's bvp4c function where the output of "bvp4c" is a structure that comprises the numerical solution and the mesh chosen by the algorithm. The study findings are given in a graphical and tabular fashion, with an emphasis on the mathematical components of the model and their influence on velocity, temperature and other physical interest aspects. The "bvp4c" solver transforms the system of equations into first-order differential equations:

Therefore, we propose the following substitutions:

$$\begin{cases} \gamma_1 = f, \gamma_2 = f', \gamma_3 = f'', \gamma\gamma_a = f''', \\ \gamma_4 = \theta, \gamma_5 = \theta', \gamma\gamma_b = \theta''. \end{cases} \tag{13}$$

Using the above-mentioned replacements, Eqs.. (7) and (8) are expressed as follows:

$$\gamma\gamma_a = \left(\frac{1}{\varphi_2\left(1+\frac{1}{B}\right)}\right)\left[F_s\gamma_2^2 - \varphi_1\left(\gamma_1\gamma_3 - \gamma_2^2\right) - \varphi_3 M(E-\gamma_2) + \frac{\varphi_2}{Da}\gamma_2\right], \tag{14}$$

$$\gamma\gamma_b = \left(\frac{-1}{\varphi_5}\right)\left[\mathrm{Pr}\varphi_4\gamma_1\gamma_5 + \varphi_3 M(Ec)(\gamma_2 - E)^2 + \varphi_2 \mathrm{Pr}(Ec)\left(1+\frac{1}{B}\right)\gamma_2^2\right]. \tag{15}$$

Corresponding BCs (10) are converted as:

Fig.4. Variation of $f'(\eta)$ vs. M.

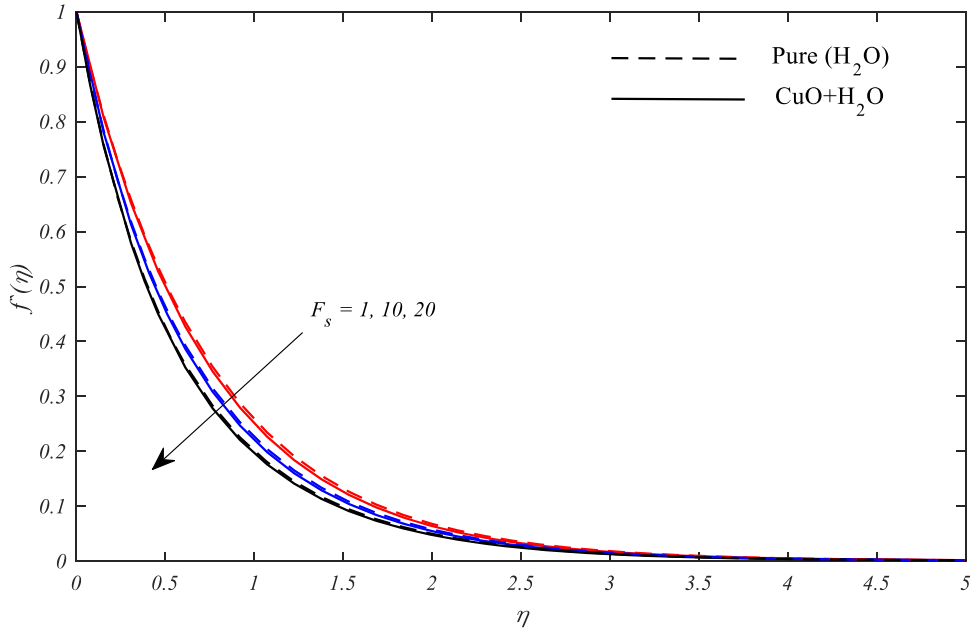

Fig.5. Variation of $f'(\eta)$ vs. F_s.

Fig. 5. Variation of $f'(\eta)$ vs. F_s.

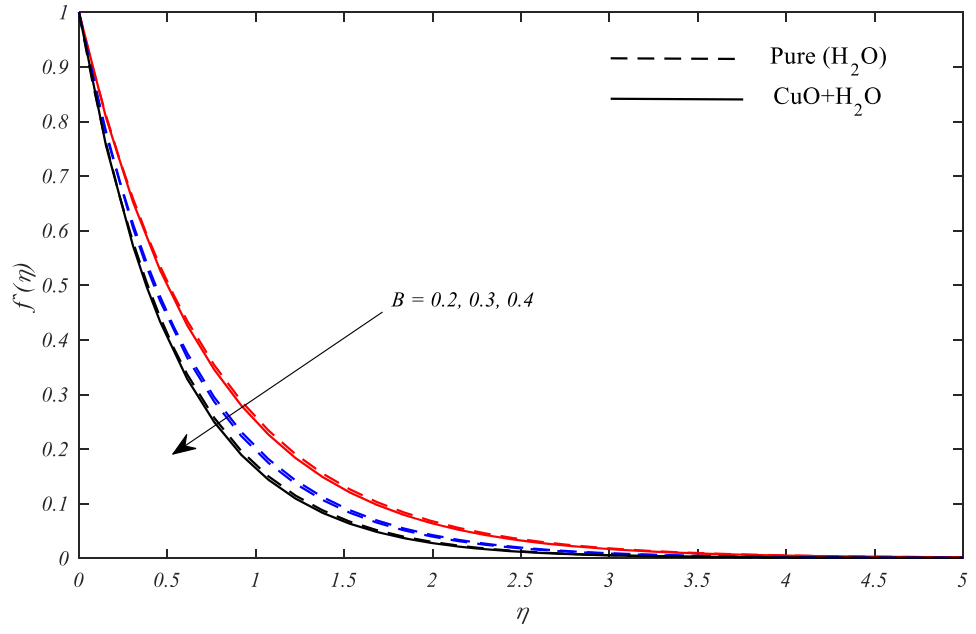

Fig. 6. Variation of $f'(\eta)$ vs. B.

$$\begin{cases} \gamma_1(0), \\ \gamma_2(0) - 1, \\ y_2(\infty), \end{cases} \qquad (16)$$

$$\begin{cases} \gamma_5(0) + 1 + \frac{\varphi_5}{Bi}\gamma_4, \\ \gamma_4(\infty). \end{cases}$$

The numerical simulations for various physical phenomenon parameters were performed for the correct computational domain [0,15] rather than [0, ∞], where the value was set at 15 since there is no more variation in the results at $\eta = 15$. The halting conditions for the iterative procedure were 10^{-4}, bvp4c is an outstanding solver for a system of ODEs when compared to other boundary value problem solvers. It is easy to set up in MATLAB and has a low computational cost, see Fig 2.

4. Results and discussion

The influence of the model parameters namelly, magnetic field M, electric filed E, volume fraction of nanoparticles χ, with range $0 \leq \chi \leq 0.2$, Forchheimer number F_s, Casson parameters, B, Biot numbers Bi, Eckert number Ec and Darcy number Da on velocity $f'(\eta)$

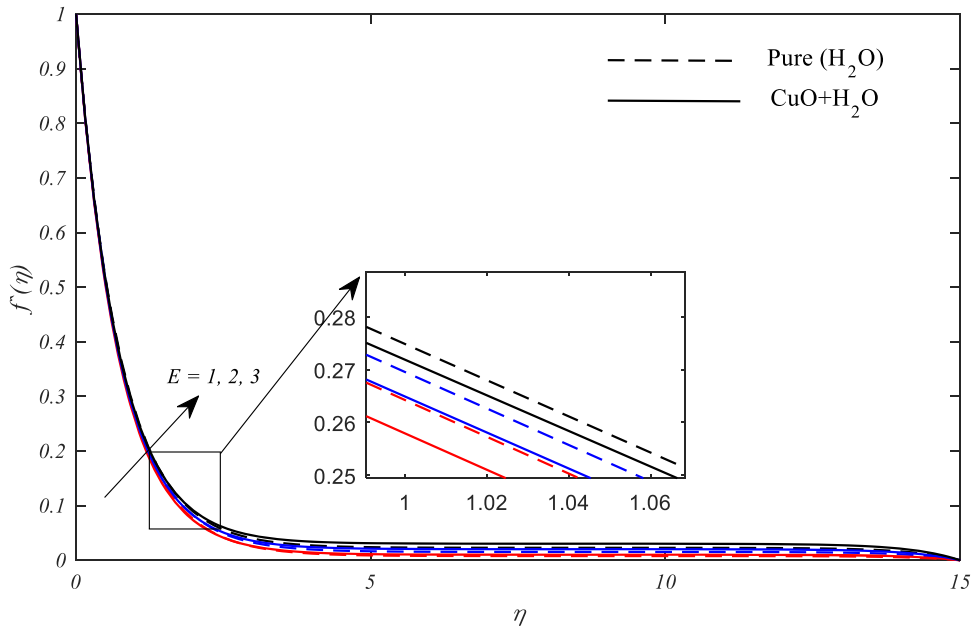

Fig. 7. Variation of $f'(\eta)$ vs. E.

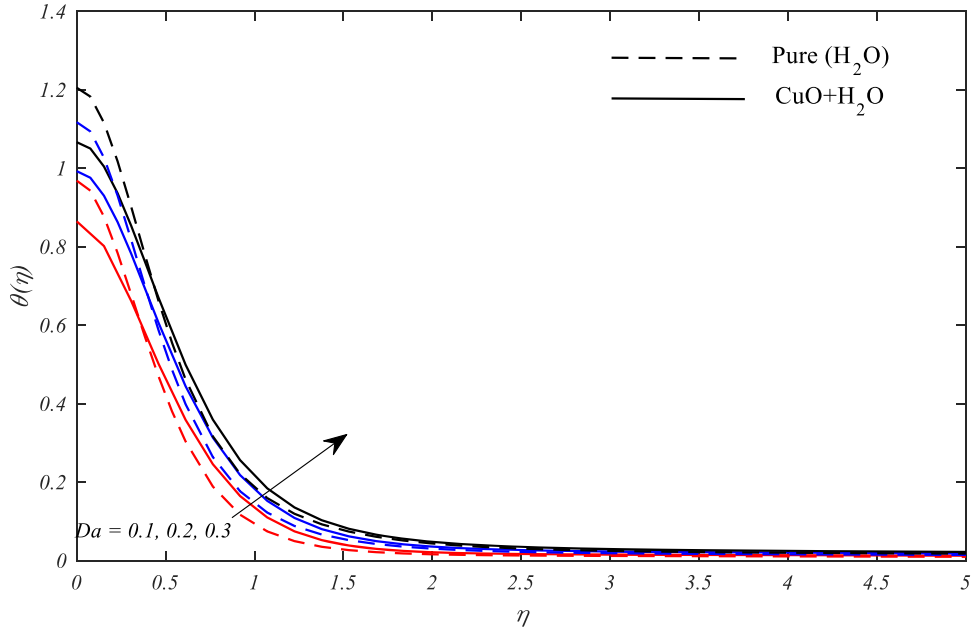

Fig. 8. Variation of $\theta(\eta)$ vs. Da.

and temperature profiles $\theta(\eta)$ are discussed viagraphical illustration as well as the computed values skin friction Cf and Nusselt number Nu for based H_2O Casson nanofluid and pure H_2O are enlisted in Tables 3 and 4. Table 1 shows the formulation of nanofluid characteristics that was used.

To establish the accuracy of the computational scheme, a comparison was made for the numeric data of skin friction coefficient and heat transfer rate with the results from other studies, such as Hafez et al.[26] . These comparisons are depicted in Table 2, which demonstrate an outstanding agreement between the present numerical results and the experimental data. This agreement provides confidence in the numerical outcomes.

The variation of the $f'(\eta)$ profiles with the alteration in the Darcy number (Da) is depicted in Fig 3. It was discovered that: the promoting the values of Da increased the velocity profile. In a sheet that was shrinking, the velocity and momentum boundary-layer's thickness grew as well, as shown in Fig 3. These findings suggest that the Darcy number is a dimensionless quantity that characterizes the permeability of a porous medium relative to its viscosity. A higher (Da) typically implies better permeability and reduced resistance to flow, which contributes to enhanced velocities in the boundary layer.

The evolution of the distributions of $f'(\eta)$ due to changing magnetic parameter (M) values is illustrated in Fig 4. It is observed that an increase in the M gives rise to a decrease in the velocity. The retarding action of the Lorentz force inflates with a rise in values of M, which affects the velocity in the boundary-layer flow of a fluid over a shrinking sheet. These findings suggest that the magnetic parameter M plays a significant role in shaping the velocity profiles in this figure.

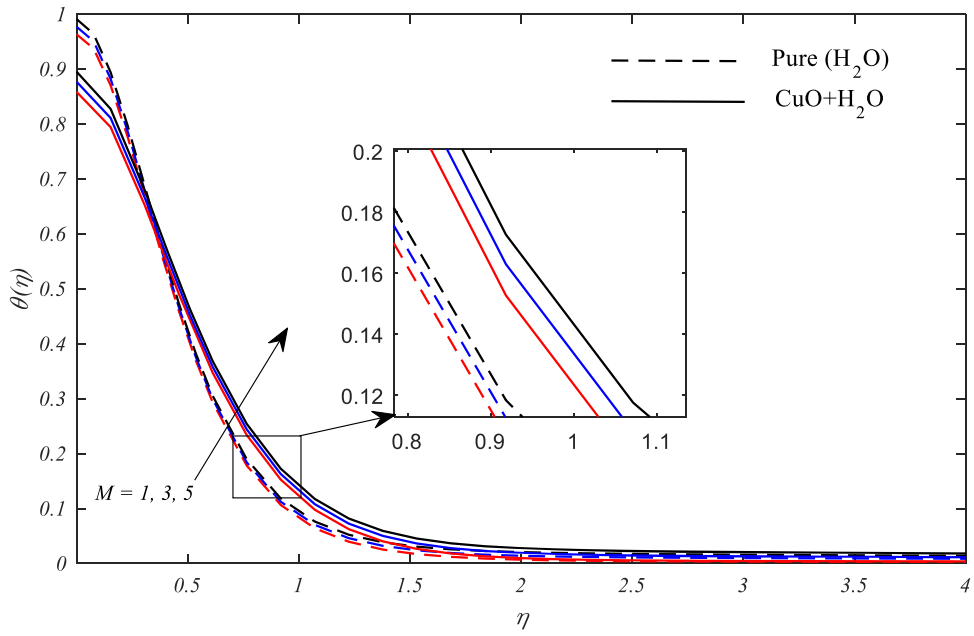

Fig. 9. Variation of $\theta(\eta)$ vs. M.

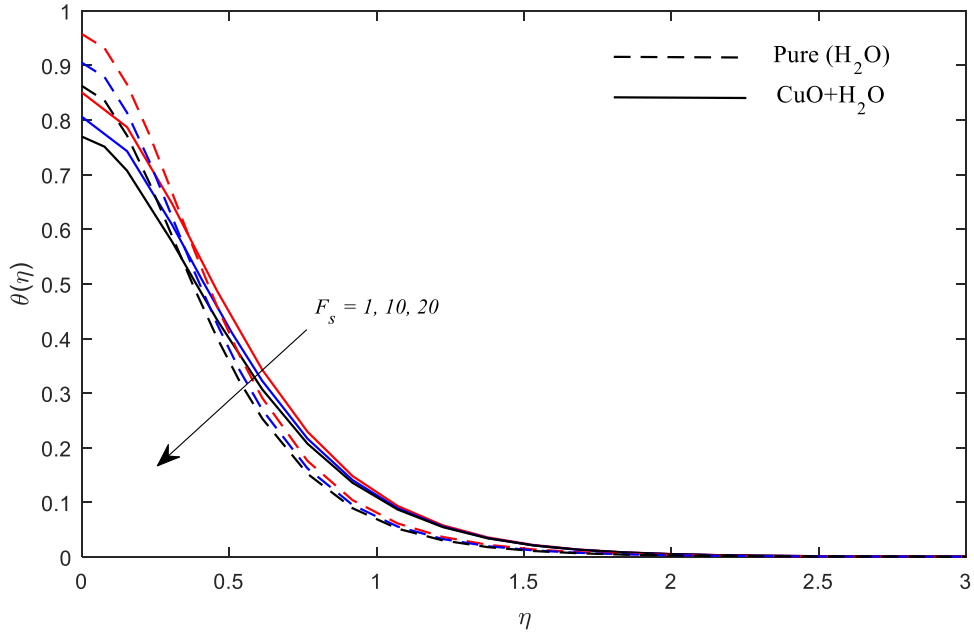

Fig.10. Variation of $\theta(\eta)$ vs. F_s.

Fig. 10. Variation of $\theta(\eta)$ vs. F_s.

Furthermore, Fig. 5 shows that the velocity profile decreases as the Forchheimer number F_s, increases. Increasing F_s, physically increases the thickness of the momentum boundary layer as well as the velocity estimate. This indicates that higher values of F_s lead to greater resistance to flow due to non-linear drag effects associated with porous media.

The influence of the Casson parameter B on the velocity profile is depicted in Fig 6. An increase in B leads to a decrease in the primary velocity and its associated layer thickness. This is due to the fact that an increase in the Casson parameter causes a reduction in the yield stress, which in turn hinders the fluid motion in the η-direction. Additionally, The impact of the electric parameter E on velocity is shown in Fig 7. It is found that as the value of the electric field parameter decreases, the boundary layer velocity increases. According to Figs 3-7, pure water has a larger velocity than copper oxide with water as the base casson nanofluid.

Figs. (8–14) show the effect of the Darcy number Da, magnetic field M, Forchheimer number F_s, Casson parameters B, Eckert number Ec, electric filed E and volume fraction of nanoparticles χ, on temperature profiles $\theta(\eta)$, respectively. According to the search results, an increase in the Darcy number is expected to decrease the amount of heat transfer from the plate to the fluid, which in turn increases the temperature of the fluid at any given point over the sheet. This is supported by Fig. 8, which determines the impression of Darcy number Da on the temperature profile θ. The search results also suggest that the effect of the Darcy number on heat transfer and temperature is influenced by other factors, such as the Rayleigh number and the geometry of the system. Fig. 9

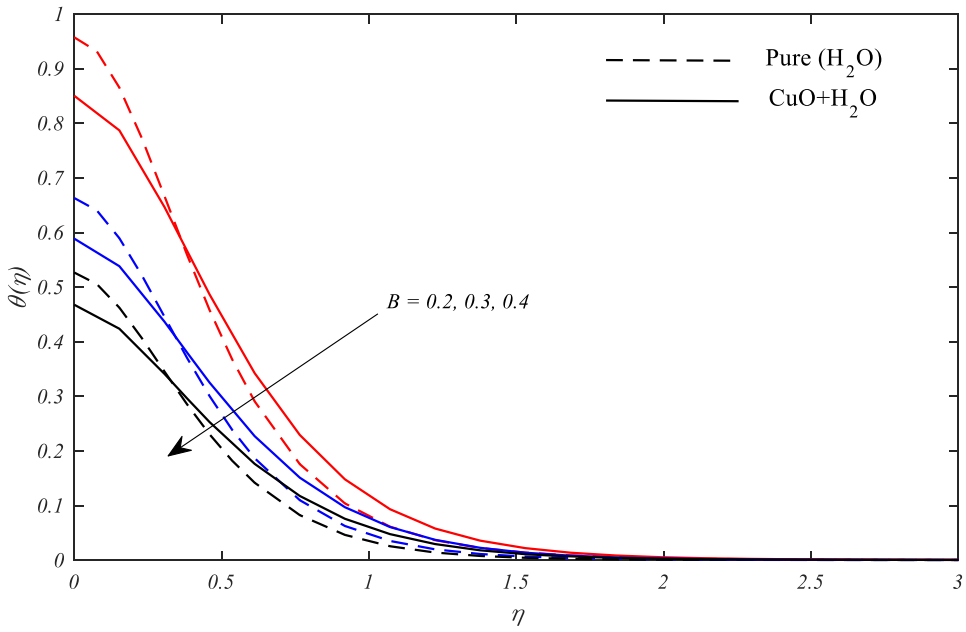

Fig. 11. Variation of $\theta(\eta)$ vs. B.

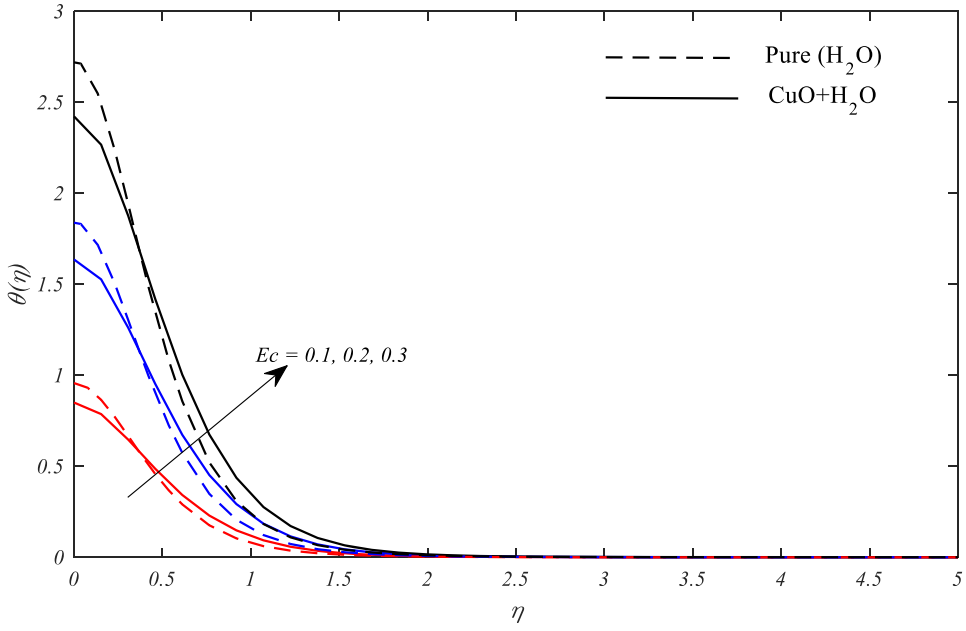

Fig. 12. Variation of $\theta(\eta)$ vs. Ec.

indicates that larger values of the magnetic parameter M contribute to an increase in temperature within the fluid. The magnetic field affects the flow characteristics and can enhance thermal energy transfer due to induced currents, which may lead to heating effects.

Fig. 10 witnesses the reduction in temperature at a large value of the Forchheimer number F_s. Physically, the reduction in temperature at a large value of the Forchheimer number F_s is primarily due to the decrease in velocity (see Fig. 5), which leads to a reduction in the fluids kinetic energy and, consequently, a decrease in temperature. A similar decreasing trend in temperature is noticed in Fig. 11 at higher values of the Casson fluid parameter β. By boosting β, the yield stress becomes less. The Casson parameters are crucial in defining the non-Newtonian behavior of the fluid. Higher values of these parameters typically correlate with increased viscosity, which can impact on temperature profiles significantly.

Fig 12 represents the influence of the Eckert number Ec on the temperature profile, showing that the increasing value of the Eckert number Ec increases the temperature profile. The Eckert number expresses the relationship between the kinetic energy in the flow and the conversion of kinetic energy into internal energy by work done against the viscous forces. This is consistent with the understanding that the presence of viscous dissipation effects significantly increases the temperature. At higher values of the electric parameter E, Fig. 13 displays a similar increasing trend in the temperature profile. This increase can be attributed to the enhanced viscous heating, reduced momentum layer thickness, thermo-migration, and increased thermal conductivity of the Casson nanofluid.

Fig. 14 indicates that the effect of χ on temperature escalates with an

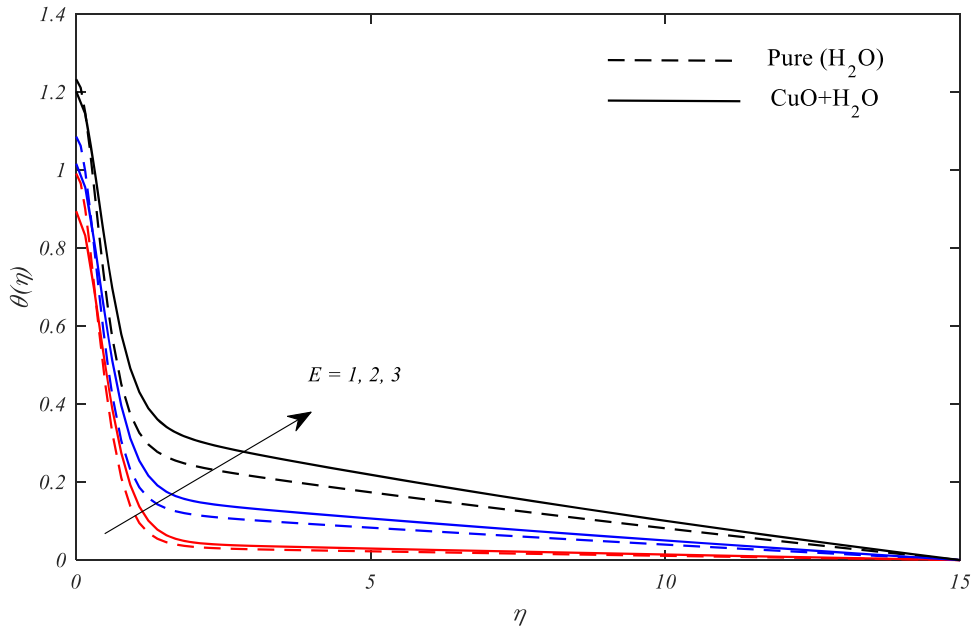

Fig. 13. Variation of $\theta(\eta)$ vs. E.

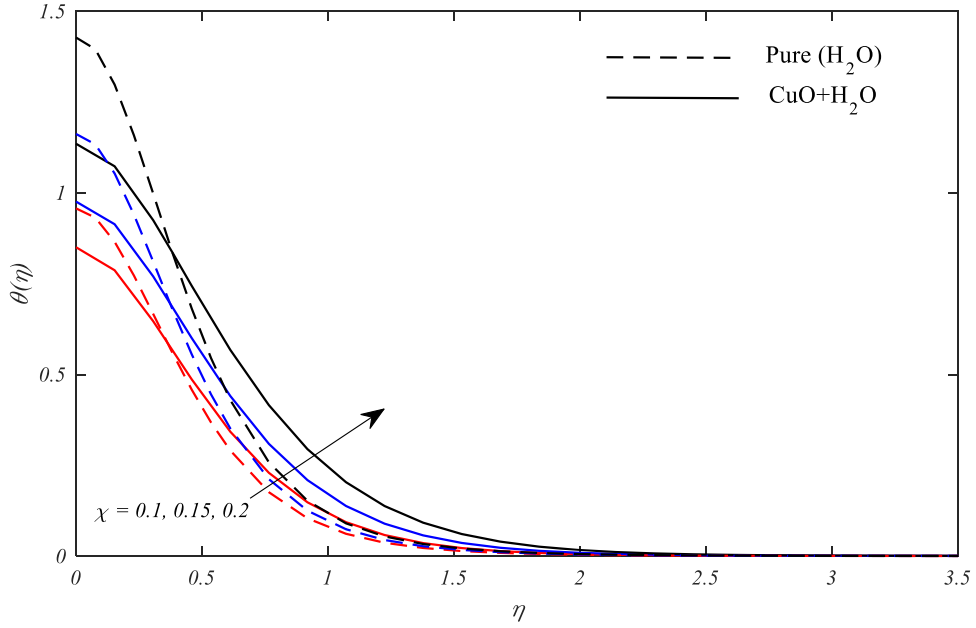

Fig. 14. Variation of $\theta(\eta)$ vs. χ.

increase in the volumetric fraction of nanoparticles due to the higher thermal conductivity of nanoparticles. As the concentration of nanoparticles increases, the thermal conductivity of the fluid increases, leading to a higher fluid temperature. The escalating volume fraction of nanoparticles greatly enhances the fluid's thermal conductivity, resulting in an increase in temperature. However, the presence of nanoparticles also increases the thermal conductivity of the fluid, resulting in higher fluid temperature. Therefore, the effect of χ on temperature escalates with an increase in the volumetric fraction of nanoparticles due to the higher thermal conductivity of nanoparticles. From Figs. (8–14), temperature profile $\theta(\eta)$ behaviour is illustrated for CuO+ H_2O—Casson nanofluid and pure Casson fluid, with a particular choice of parameters. As can be seen, the growth of $\theta(\eta)$ is resulting in CuO+H_2O—Casson nanofluid compared to pure water. Overall, the behavior of temperature profile $\theta(\eta)$ for CuO+H_2O—Casson nanofluid and pure Casson fluid demonstrates the potential of nanofluids in improving heat transfer and fluid flow application.

Tables 3 and 4 provided a detailed analysis of the impacts of various physical parameters on the values of skin friction coefficient $\sqrt{Re_x}Cf$ and Nusselt number $\frac{-Nu}{\sqrt{Re_x}}$ for based H_2O Casson nanofluid and pure H_2O. The numerical values of the skin friction coefficient $(-\sqrt{Re_x}Cf)$ are enhanced by increased values of the magnetic parameter (M), Forchheimer number (F_s), and volume fraction of nanoparticles. On the other hand, $(-\sqrt{Re_x}Cf)$ reduces with an enhanced Darcy number (Da), Casson parameter (β), and electric field parameter (E) . As the values of Da, M, Biot number (Bi), Eckert number (Ec), and electric field parameter (E) increase, the Nusselt number's $\frac{-Nu}{\sqrt{Re_x}}$ numerical results also increase and show different patterns for rising values of F_s. Overall, the numerical values of the friction factor and Nusselt number are affected

Table 3
Variations in $\left(-\sqrt{Re_x}\,Cf\right)$ between pure H_2O and ($CuO+H_2O$) at various parameters.

Da	*M*	*Fs*	*B*	*E*	χ	Pure H_2O	$CuO+H_2O$
0.1	0.1	1	0.2	0.1	0.2	14.1174	14.6148
0.2						10.3796	11.0456
0.3						8.7867	9.5634
	0.1					14.1174	14.6148
	0.3					14.1766	14.7142
	0.5					14.2355	14.8130
		1				14.1174	14.6148
		10				16.1896	16.6210
		20				18.2184	18.6000
			0.2			14.1174	14.6148
			0.3			11.9975	12.4202
			0.4			10.7824	11.1622
				0.1		14.1174	14.6148
				0.3		14.1024	14.5890
				0.5		14.0874	14.5632
					0.1	10.6982	10.9037
					0.15	12.2308	12.5556
					0.2	14.1174	14.6148

Table 4
Variations in $\frac{-Nu}{\sqrt{Re_x}}$between pure H_2O and ($CuO+H_2O$) at various parameters.

Da	*M*	*Bi*	*Fs*	*Ec*	*E*	Pure H_2O	$CuO+H_2O$
0.1	0.1	0.1	1	0.1	0.1	0.0428	0.0135
0.2						0.0657	0.0302
0.3						0.0794	0.0400
	0.1					0.0428	0.0135
	0.3					0.0429	0.0138
	0.5					0.0431	0.0140
		0.1				0.0428	0.0135
		0.5				0.1590	0.0543
		1				0.2407	0.0869
			1			0.0428	0.0135
			10			0.0363	0.0088
			20			0.0308	0.0047
				0.1		0.0428	0.0135
				0.2		0.1769	0.1209
				0.3		0.3111	0.2282
					0.1	0.0428	0.0135
					0.3	0.0431	0.0141
					0.5	0.0437	0.0151

by various dimensionless parameters, including the magnetic parameter, Forchheimer number, volume fraction of nanoparticles, Darcy number, Casson parameter, electric field parameter, Biot number, and Eckert parameter. The numerical analysis reported in the study indicates that the $CuO+H_2O$ Casson nanofluid exhibits the largest skin friction coefficient effects compared to pure H_2O, as shown in Table 3. This suggests that the addition of CuO to water increases the skin friction coefficient. On the other hand, the Nusselt number for pure water is higher than that for the $CuO+H_2O$ Casson nanofluid, as shown in Table 4, indicating that the heat transfer rate is higher for pure water compared to the nanofluid. The research provides insights into the behavior of Casson nanofluids, specifically in terms of skin friction and heat transfer characteristics. The findings are valuable for understanding the impact of nanofluids on fluid dynamics and heat transfer processes.

5. Conclusions

This study uses the bvp4c solver to numerically resolve a stable two-dimensional Casson Nanofluid Darcy-Forchheimer boundary layer with convective boundary conditions by stretching the sheet surface via a porous medium and applying an electric MHD. The following is an explanation of the main observations:

- The velocity profile of the Casson nanofluid decreases with increasing values of the Casson parameter, magnetic parameter, and Forchheimer number. Conversely, an increase in the electric parameter and Darcy number leads to an enhancement in the velocity profile.
- The temperature profile is positively influenced by higher values of the Darcy number, magnetic parameter, Eckert parameter, electric parameter, and volume fraction of nanoparticles. In contrast, increases in the Forchheimer number and Casson parameter result in a reduction of the temperature profile.
- There is a significant increase in the skin friction coefficient with rising values of the magnetic parameter, Forchheimer number, and volume fraction of nanoparticles. However, it decreases when the Darcy number, electric parameter, and Casson parameter are increased.
- The Nusselt number increases with higher values of the Darcy number, magnetic parameter, Biot number, Eckert number, and electric field parameter. In contrast, the Nusselt number decreases as the Forchheimer number increases.
- Pure water exhibits a higher velocity and Nusselt number compared to copper oxide-water-based Casson nanofluid. Conversely, copper oxide shows higher temperature and skin friction coefficients under similar conditions.

The electric MHD Darcy-Forchheimer flow is a topic of active research, with several studies investigating its implications for different types of nanofluid flow. The combination of the Darcy-Forchheimer model with MHD and electrical effects is of interest in understanding the behavior of fluids in porous media under the influence of electromagnetic forces.

6. Future perspectives

The Finite Element Method, Chebyshev Spectral Method and Keller-Box Scheme present promising numerical approaches for addressing a variety of potential applications. These techniques can be effectively utilized in fields such as bioinformatics, fluid mechanics, and financial mathematics, where they hold significant implications for advancing research and practical solutions.

Declaration of competing interest

There is no conflicts of interest of my paper.

Acknowledgement

Author is grateful to acknowledge the Ajloun National University for providing the facilities support.

Data availability

No data was used for the research described in the article.

References

1. Patil MB, Shobha K, Bhattacharyya S, Said Z. Soret and Dufour effects in the flow of Casson nanofluid in a vertical channel with thermal radiation: entropy analysis. *J Therm Anal Calorim*. 2023;148:2857–2867.
2. Liu H, Lan L, Abrigo J, et al. Comparison of Newtonian and non-Newtonian fluid models in blood flow simulation in patients with intracranial arterial stenosis. *Front Physiol*. 2021;12, 718540.
3. Casson N. Flow equation for pigment-oil suspensions of the printing ink-type. *Rheol Disperse Syst*. 1959:84–104.
4. Alkasasbeh H. Numerical solution of heat transfer flow of casson hybrid nanofluid over vertical stretching sheet with magnetic field effect. *CFD Letters*. 2022;14:39–52.
5. Alwawi FA, Hamarsheh AS, Alkasasbeh HT, Idris R. Mixed convection flow of magnetized Casson nanofluid over a cylindrical surface. *Coatings*. 2022;12:296.
6. Alwawi FA, Alkasasbeh HT, Rashad AM, Idris R. A numerical approach for the heat transfer flow of carboxymethyl cellulose-water based Casson nanofluid from a solid

sphere generated by mixed convection under the influence of Lorentz force. *Mathematics*. 2020;8:1094.
7. Choi SU, Eastman JA. *Enhancing Thermal Conductivity of Fluids With Nanoparticles*. Argonne, ILUnited States: Argonne National Lab.(ANL); 1995.
8. Yang J, Yang X, Wang J, Chin HH, Sundén B. Review on thermal performance of nanofluids with and without magnetic fields in heat exchange devices. *Front Energy Res*. 2022;10, 822776.
9. Pavithra K, Parol V, Brusly Solomon A, Yashoda M. Investigation of thermal conductivity and thermal performance of heat pipes by structurally designed copolymer stabilized ZnO nanofluid. *Sci Rep*. 2023;13:14219.
10. Kaggwa A, Atkins M, Tarighaleslami A, Walmsley M, Carson JK. Thermal Performance of Selected Nanofluids with Surfactants. *Int J Thermophys*. 2023;44:160.
11. Irfan M, Farooq MA, Iqra T. A new computational technique design for EMHD nanofluid flow over a variable thickness surface with variable liquid characteristics. *Front Phys*. 2020;8:66.
12. Algehyne EA, Alharbi AF, Saeed A, Dawar A, Kumam P, Galal AM. Numerical analysis of the chemically reactive EMHD flow of a nanofluid past a bi-directional Riga plate influenced by velocity slips and convective boundary conditions. *Sci Rep*. 2022;12:15849.
13. Ali A, Khan HS, Saleem S, Hussan M. EMHD nanofluid flow with radiation and variable heat flux effects along a slandering stretching sheet. *Nanomaterials*. 2022;12:3872.
14. Lanjwani HB, Saleem S, Chandio MS, Anwar MI, Abbas N. Stability analysis of triple solutions of Casson nanofluid past on a vertical exponentially stretching/shrinking sheet. *Adv Mech Eng*. 2021;13, 16878140211059679.
15. Lanjwani H, Kamboh S, Anwar M, Alahmadi H, Ambreen T, Shehzad S. Stability analysis of stratified radiative non-Newtonian Casson nanofluid flow past on stretching/shrinking sheet using two-phase model. *Chin J Phys*. 2023;85:752–775.
16. Basha HT, Sivaraj R. Stability analysis of casson nanofluid flow over an extending/contracting wedge and stagnation point. *J Appl Computat Mech*. 2022;8:566–579.
17. El-Zahar ER, Mahdy AEN, Rashad AM, Saad W, Seddek LF. Unsteady MHD mixed convection flow of non-Newtonian Casson hybrid nanofluid in the stagnation zone of sphere spinning impulsively. *Fluids*. 2021;6:197.
18. Sangeetha E, De P. Bioconvective Casson nanofluid flow toward stagnation point in non-Darcy porous medium with buoyancy effects, chemical reaction, and thermal radiation. *Heat Transfer*. 2023;52:1529–1551.
19. Sangeetha E, De P. Darcy– Forchheimer porosity effects on nanofluid with motile gyrotactic microorganisms over convectively heated surface. *Nanosci Technol*. 2021;12.
20. Sangeetha E, De P. Bioconvection in nanofluid flow embedded in non-Darcy porous medium with viscous dissipation and Ohmic heating. *J Porous Media*. 2021:24.
21. Jawad M, Saeed A, Kumam P, Shah Z, Khan A. Analysis of boundary layer MHD Darcy-Forchheimer radiative nanofluid flow with soret and dufour effects by means of marangoni convection. *Case Stud Thermal Eng*. 2021;23, 100792.
22. Li S, Raghunath K, Alfaleh A, et al. Effects of activation energy and chemical reaction on unsteady MHD dissipative Darcy–Forchheimer squeezed flow of Casson fluid over horizontal channel. *Sci Rep*. 2023;13:2666.
23. Butt ZI, Ahmad I, Shoaib M, Ilyas H, Raja MAZ. Electro-magnetohydrodynamic impact on Darrcy-Forchheimer viscous fluid flow over a stretchable surface: integrated intelligent Neuro-evolutionary computing approach. *Int Commun Heat Mass Transfer*. 2022;137, 106262.
24. Lund LA, Chandio AF, Vrinceanu N, Yashkun U, Shah Z, Alshehri A. Darcy–Forchheimer magnetized nanofluid flow along with heating and dissipation effects over a shrinking exponential sheet with stability analysis. *Micromachines (Basel)*. 2022;14:106.
25. Abbas A, Jeelani MB, Alharthi NH. Darcy–Forchheimer relation influence on MHD dissipative third-grade fluid flow and heat transfer in porous medium with joule heating effects: a numerical approach. *Processes*. 2022;10:906.
26. Hafez N, Thabet EN, Khan Z, Abd-Alla A, Elhag S. Electroosmosis-modulated Darcy–Forchheimer flow of Casson nanofluid over stretching sheets in the presence of Newtonian heating. *Case Stud Thermal Eng*. 2024;53, 103806.
27. El-Kabeir S, El-Hakiem M, Rashad A. Group method analysis of combined heat and mass transfer by MHD non-Darcy non-Newtonian natural convection adjacent to horizontal cylinder in a saturated porous medium. *Appl Math Model*. 2008;32:2378–2395.
28. Murthy P, RamReddy C, Chamkha A, Rashad A. Magnetic effect on thermally stratified nanofluid saturated non-Darcy porous medium under convective boundary condition. *Int Commun Heat Mass Transfer*. 2013;47:41–48.